Technium Electro

Technium Electro Vol. 1, pp.53-68 (2023)
ISSN:3008-6795
www.techniumscience.com

Mixed alkali effect as a tunable way of controlling the electrical and optical properties of manganese phosphate glasses

Sana Bahrami,[1] Majid Karimi[2, 3]

Abstract

The mixed alkali effect (MAE) can be utilized in tuning various properties of oxide glasses. In this paper, MAE was explored in the electrical and optical properties of new manganese phosphate glasses with the composition $40P_2O_5$–$10MnO_2$–(50-x)Li2O–xRb_2O, x= 5, 15, 25, 35, and 45 mol %. Glassy samples were prepared by the conventional melt quenching technique. It was observed that the conductivity in the present glassy system is more ionic rather than electronic. Due to the presence of the MAE, the activation energy varied nonlinearly with Rb_2O molar percentage and reached a maximum of 0.93 eV at x= 25 mol%. The optical properties also showed nonlinear variation with Rb_2O content, which supported the existence of the MAE in the optical properties.

Keywords: Mixed alkali effect; Phosphate glasses; Transition metal ions; Activation energy; UV–Vis spectroscopy; Optical bandgap

1. Introduction

P_2O_5 is one of the four classic Zachariasen glass-forming oxides along with SiO_2, GeO_2 and B_2O_3. Phosphate-based glasses have attracted the attention of many researchers due to their technological and biological applications, as well as their unique physical properties such as simple structure, strong glass-

1 Sahand University of Technology, Tabriz, Iran.

2 University of Tabriz, Tabriz, Iran.

3 E-mail: majidkarimi@tabrizu.ac.ir.

Technium Electro Vol. 1, pp.53-68 (2023)
ISSN:3008-6795
www.techniumscience.com

forming characteristic, UV transmission and optical features, low melting point and glass transition temperatures, large thermal expansion coefficients, and biomedical compatibility [1]. These glasses are being used as host materials for lasers, as potential cathode materials in Li-ion batteries, optical filters, and also to store nuclear waste. They can also be employed in biological applications if properly doped with suitable elements. In pure phosphate glass, moisture can interact with P-O bonds, forming phosphoric acid and lowering the system's chemical durability. However, it has been demonstrated that adding some alkali/alkaline oxides, transition metal ions (TMIs), or second glass-forming oxide can remarkably improve chemical durability as well as thermal and mechanical stability of pure phosphate glasses [2]. P_2O_5 glasses are composed of tetrahedral PO_4^{3-} units with three bridging oxygen atoms and one non-bridging oxygen atom (NBO). The PO_4^{3-} units are joined by bridging oxygen atoms. The addition of a modifier oxide into the phosphate glass network causes it to depolymerize. The presence of additional oxygen atoms introduced by the modifying oxides results in the formation of negative non-bridging oxygen sites. The positive charges of the modifying cations balance out these negative charges.

Many glassy networks containing alkali elements have exhibited a nonlinear behavior of physical properties by gradually replacing one alkali element with another one [3, 4]. This phenomenon is well-known as the mixed alkali effect (MAE). MAE gives rise to large changes in properties that are associated with ionic transport, such as electrical conductivity, activation energy, dielectric loss, glass transition temperature, internal friction, viscosity and density. The order of departure from linearity depends on the total alkali elements concentration, the size and mass difference of alkali elements, and the temperature of observation [5]. In general, the MAE becomes stronger with an increase in total alkali elements concentration and mismatch of alkali elements size; it becomes weaker at higher temperatures [6, 7]. It should be mentioned that MAE is only detectable when the total alkali concentration is higher than ~10 mol%. This phenomenon is not limited to non-crystalline systems and has also been observed in crystalline ion conductors.

The mixed alkali effect can be used in tailoring favorable properties of different oxide glasses. So far, many theories and models have been proposed to explain the origin of this intriguing effect. However, little research has been conducted on mixed alkali glasses incorporating TIMs. The present work was carried out to investigate the MAE in the electrical and optical properties of new compositions of multifunctional phosphate glasses containing MnO_2.

Technium Electro Vol. 1, pp.53-68 (2023)
ISSN:3008-6795
www.techniumscience.com

2. Experimental

The conventional melt quenching technique was used to prepare the glass composition of $40P_2O_5$–$10MnO_2$–$(50-x)Li_2O$–xRb_2O with x= 5, 15, 25, 35, and 45 mol%. Because of the high hygroscopicity and volatile nature of phosphorus pentoxide, lithium oxide and rubidium oxide, $NH_4H_2PO_4$, Li_2CO_3, Rb_2CO_3, and MnO_2 were taken as starting materials. CAS registry number, supplier and purity of the chemicals are provided in Table 1. Convenient amounts of initial materials were weighed and grounded by a pestle in an alumina crucible, until getting a homogeneous mixture. The crucible was placed in an electrical furnace and kept for 2 hours at ~420 °C to complete initial reactions and remove volatile components from the composition. Then, the furnace temperature was slowly increased up to the melting point of each glass composition (between 870 and 970 °C). After one hour the melt was poured on a preheated stainless-steel plate into an annealing furnace. The obtained samples were annealed for 3h near the glass transition temperature to relieve the mechanical and thermal stresses resulting from the quenching. Also, by immersing the end of an alumina tube into the molten material and steadily blowing through the alumina tube, thin blown films of the samples were prepared.

To confirm the amorphous nature of the glasses, X-ray diffractometry (XRD) was carried out by a Bruker–D8 Advance X-ray diffractometer with a scanning angle (2θ) of 10° to 120°. The standard two-probe method was employed to measure dc electrical conductivity. To do this, the prepared bulk samples were first polished by several grads of polishing papers, and then a silver paste coating was applied to both sides of the samples to serve as electrodes. After polishing, the samples have flat circular surfaces with diameters of ~19 mm and a thickness of ~ 1.2 mm. The silver electrodes have also a circular cross-section with a diameter of ~ 13 mm and a thickness of ~ 120-130 μm. We used the guard ring method to prevent the influence of surface currents in the measurements. The samples were heated up from 297 K to 397 K with a temperature step of 10 K. Temperature was measured with an accuracy of 1 K using a chromel-alumel thermocouple. At eleven specific temperatures, the current-voltage characteristics were investigated for each of the samples in the voltage range of 10–300 V. The current and voltage were measured using a digital picometre (DPM-111 Scientific Instruments, Roorkee) and a multi-meter with an accuracy of ±10 mV. The conductivity (σ) has been determined using the relation $\sigma = 1/\rho$, where $\rho = (RA)/t$ is the resistivity and t, R and A are the thickness, resistance, and cross-sectional area of the sample, respectively. The uncertainty in the measurement of dc electrical conductivity has been determined to be approximately ± 5%. The optical absorption and reflectance spectra were recorded at room temperature for all the samples in the wavelength region of 200-900nm using a standard UV-Vis spectrophotometer manufactured by Scinco.

Technium Electro Vol. 1, pp.53-68 (2023)
ISSN:3008-6795
www.techniumscience.com

3. Results and discussion

Figure 1 shows the XRD patterns of the samples. As can be seen, the obtained patterns comprised only broad humps, which is typical of vitreous solids. There is no intense Bragg peak in the spectra, except for short range-related broad peaks at small angles. This corroborates the lack of crystalline characteristics, implying that all prepared samples have an amorphous nature.

Figure 2 illustrates the I–V characteristics of the samples at 297 and 347 K. All the prepared glasses exhibit ohmic behavior within the voltage range of 10– 300 V. The logarithm of dc electrical conductivity (Lnσ) was then plotted versus reciprocal temperature ($1/k_BT$) (see Fig. 3). As is clear, the dc electrical conductivity of all samples increases with rising temperature. According to the Arrhenius equation, the negative slopes of the linear fits of the plots gives the values of activation energy:

$$\sigma = \sigma_0 \, exp\left(\frac{-W}{k_B T}\right) \qquad (1)$$

In Eq. (1), σ is the electrical conductivity, σ_0 is a constant, and k_B is the Boltzmann constant. The error in the estimation of activation energy is approximately ±0.01 eV. The calculated values of Lnσ and W are given in Table 2. Figures 4 and 5 represent the variation of Lnσ and W as a function of Rb_2O content, respectively. The nonlinear behavior of activation energy and dc electrical conductivity is due to the existence of MAE. From Fig. 4, the dc conductivity initially decreases with increasing Rb_2O molar percentage (from x = 5% mol to x = 25%mol) and reaches a minimum at x = 25%mol; with a further increase of the Rb_2O content, dc conductivity increases. Activation energy varies in reverse order; it first increases from x = 5% mol to x = 25%mol, reaches a maximum at x = 25% mol and then decreases (see Fig. 5). The electrical properties of all materials depend on their structures. Although P_2O_5 does not play a major role in electrical conductivity, the structural phosphate units have an important contribution to the conductivity of phosphate glasses. Mn/P and O/ (Mn + P) ratios are constant in our samples. Thus, it can be assumed that the structural units of MnO_2 in the vitreous networks dose not influence the variation of electrical properties of the samples. However, in oxide glasses, depending on host glass composition and preparation conditions, manganese might exist in more than one valence state [3]. In this case, electron transfer between manganese ions with two different oxidations is possible. Therefore, the electronic conductivity can occur between the valance states by small polaron hopping. However, it has been shown that for mixed alkali glasses with high total alkali concentration, the electrical conductivity arising from the inter-valence transfer process between TIMs can be neglected [8]. When the glasses become increasingly oxygen-donor, the formation of the higher oxidation valence state is favored. Thus, it can be said that in our glassy system, electrical conductivity is more ionic rather than electronic, and the minimum dc conductivity is associated with the mixed

alkali effect on the ionic conductivity. Two well-known descriptions of the MAE in electrical conductivity are the dynamic structure model (DSM) [9 -11], and the random ion distribution model (RIDM) [4, 12, 13]. The DSM assumes that in a mixed alkali glass, A and B ions form their local environments, which are distinct for different ions. This results in a site energy mismatch, and the possibility of A-B hop decreases compared to A-A or B-B hops. Therefore, diffusion occurs mainly in some preferred paths, and this is considered to be the main reason for the reduced ionic conductivity. Swenson et al. suggested that the principal origin of MAE could be described from the static structural models of real glasses. Diffraction studies and reverse Monte Carlo simulations have shown that in mixed alkali phosphate glasses, different alkali ion types have different local and composition invariant environments. The alkali ions are randomly dispersed in low dimensional pathways between the phosphate chains. The different local environments of the two types of alkali ions greatly reduce the possibility of hops to dissimilar sites, and the origin of the mixed alkali effect can be understood as a natural result of this structural arrangement. In the structure of a static glass, random mixing of alkali ions in low dimension pathways and site mismatch causes part of the preferred diffusion pathways to be blocked. This is the main basis of the RIDM random distribution model, which provides a complete structural picture of the mixed alkali glasses. In our glassy system, ionic conductivity is mainly due to the existence of lithium and rubidium alkali ions. These ions are randomly mixed so that each type of alkali ion has different conduction pathways of low dimensionality. This causes rubidium ions to block the pathways of lithium ions and vice versa. Energy mismatch between dissimilar sites reduces the hope possibility of lithium ions into rubidium sites and rubidium ions into lithium sites (compared to the possibility of lithium–lithium, and rubidium–rubidium hops). By gradually replacing lithium ions with rubidium ions, the blocking of ion hopping to a neighboring site adapted for a dissimilar ion begins and reaches a maximum at x = 25 mol%. As a result, the activation energy reaches a maximum at x = 25 and, as a result, the ionic conductivity reaches a minimum at this point. This is the main reason for the minimum dc electrical conductivity. Figure 4 displays the temperature dependence of the MAE. As can be seen, the magnitude of MAE diminishes with increasing temperature. This is a direct result of the activation energies of the mixed alkali glasses. As the temperature rises, the energy mismatch between different ionic sites decreases; it becomes comparable to K_BT at high temperatures. This reduces the magnitude of the mixed alkali effect. Lowering the temperature reduces the average hopping rate in mixed alkali glasses much more rapidly than in single alkali glasses. The partial blockage of the preferred diffusion pathways in mixed alkali glasses forces ions to move along pathways with higher energy barriers. This leads to an increase in activation energy.

Technium Electro Vol. 1, pp.53-68 (2023)
ISSN:3008-6795
www.techniumscience.com

Analysis of the optical absorption spectrum, especially the absorption edge in the ultraviolet and visible regions, is one of the most suitable tools for studying the band structure and bandgap energy in crystalline/non-crystalline systems. Figure 6 represents the optical absorption spectra of the samples.

The absence of sharp absorption edges in the spectra supports the amorphous nature of the samples [14]. The optical absorption coefficient, α(ν), was calculated from the following relation:

$$\alpha(\upsilon) = \frac{1}{d} log\left(\frac{I_0}{I_t}\right) \qquad (2)$$

where d is the thickness of the sample, and I_0 and I_t are the incident and transmitted beam intensities, respectively. The absorbance is expressed by the factor $\log(I_0/I_t)$. For amorphous materials, the absorption coefficient as a function of the incident photon energy is given by [15]:

$$\alpha(\upsilon) = \beta \frac{(h\upsilon - E_{opt})^n}{h\upsilon} \qquad (3)$$

where β is the band tailing parameter, and hν is the incident photon energy. E_{opt} represents the optical bandgap. The type of electronic transitions in k-space is determined by index n, which takes the values 2, 1/2 for indirect allowed and direct allowed transitions, respectively. Figure 7 shows the linear portion of $(\alpha h\nu)^{1/2}$ versus the incident photon energy curve for all samples. The calculated values for the optical bandgap are listed in Table 1. As can be seen, when Li_2O is replaced by Rb_2O, the indirect allowed optical bandgap values vary from 2.175 eV to 2.729 eV. The nonlinear variation of E_{opt} with Rb_2O molar percentage confirms the existence of MAE in the optical properties. The addition of network modifiers leads to the modification of the glass structure and the creation of non-bridging oxygen atoms (NBOs). In single alkali glasses, E_{opt} decreases with increasing alkali content, which is due to an increase in the formation of NBOs [16]. The nonlinear behavior of optical bandgap in our glassy samples can be attributed to a change in the formation of NBOs upon substituting Li ions with Rb ions. The maximum of E_{opt} at x = 25 mol% might be linked to a reduction in the formation of NBOs at this point. When α(ν) is between 102 and 104 cm^{-1}, there is an Urbach tail for absorption. According to Eq. 4, α(ν) depends exponentially on the photon energy [7, 17];

$$\alpha(\upsilon) = \alpha_0 \, exp\left(\frac{h\upsilon}{E_U}\right) \qquad (4)$$

where hν is the incident photon energy and α_0 is a constant. E_U (Urbach energy) represents the width of localized states tailing in the bandgap [17]. E_U values were computed from the slopes of the linear portion of Lnα versus the incident photon energy curve (see Fig. 8). The obtained values for the Urbach energy are also listed in Table 3. Figure 9 shows the compositional dependence of optical bandgap and

Technium Electro Vol. 1, pp.53-68 (2023)
ISSN:3008-6795
www.techniumscience.com

Urbach energy. E_U lies between 0.374 eV and 0.721 eV, which is comparable to the results reported for inorganic glasses. The nonlinear variation of the Urbach energy is also due to the existence of the MAE.

Figure 10 illustrates the reflectance spectra of the samples. The refractive index is an intrinsic characteristic of materials that is determined by the polarizability of ions and local fields inside the material structure. Knowing the refractive indices of optical materials opens up a world of possibilities for their use in optical devices such as window layers, switches, filters, and modulators. While the refractive index affects the propagating wave's phase, the extinction coefficient influences its amplitude. The refractive index (n) was calculated for all samples using Eq. 5 [16];

$$n = \left(\frac{1+R}{1-R}\right) + \sqrt{\frac{4R}{(1-R)^2} - k^2} \qquad (5)$$

where R represents the reflectance and $k = \alpha\lambda/4\pi$ is the extinction coefficient. Figure 11 depicts the refractive index variation with Rb_2O content. Another important parameter that reveals the light-matter interaction is the optical dielectric constant (ε), which is computed from the refractive index by using;

$$\varepsilon = n^2 \qquad (6)$$

The refractive index and dielectric constant exhibit nonlinear behavior with Rb_2O content, as seen in Table 3 and Fig. 11. This lends support to the existence of the mixed alkali effect in the optical properties of the present glassy system. These nonlinear variations may be due to a change in the formation of NBOs upon substitution of Li_2O by Rb_2O.

The reflection loss from the glass surface (R) was determined for all samples by using Fresnel's formula [18]:

$$R = \left(\frac{n-1}{n+2}\right)^2 \qquad (7)$$

Table 3 shows the values obtained for the reflection loss. As can be seen, R fluctuates nonlinearly with Rb_2O molar percentage, owing to the influence of the MAE on optical characteristics.

4. Conclusion

Manganese phosphate glasses with a composition of $40P_2O_5$–$10MnO_2$–$(50\text{-}x)Li_2O$–xRb_2O (x= 5, 15, 25, 35, and 45 mol%) were prepared and their electrical and optical characteristics were investigated for the MAE. The mixed alkali effect first manifested itself as a deep dc electrical conductivity minimum. The reason for this minimum was explained within the framework of the random ion

Technium Electro Vol. 1, pp.53-68 (2023)
ISSN:3008-6795
www.techniumscience.com

distribution model. The higher blocking of ion hopping to a neighboring site adapted for a dissimilar ion leads to higher activation energy and, as a result, a lower conductivity. The MAE was also seen in the optical properties of the present glassy system. The nonlinear variation of optical bandgap and refractive index is due to a change in the formation of non-bridging oxygen atoms. The presence of this intriguing phenomenon may be used to control different properties of mixed alkali phosphate glasses, which can be beneficial in a variety of scientific and technological applications.

References

1. J. R. V. Wazer and K. A. Holst, "Structure and Properties of the Condensed Phosphates. I. Some General Considerations about Phosphoric Acids1," *J. Am. Chem. Soc.*, **72**(2), 639-644 (1950).
2. A. Chahine *et al.*, "Effect of CuO on the structure and properties of (50− x/2) Na2O□ xCuO□(50− x/2) P2O5 glasses," *Mater. Chem. Phys.*, **84**(2-3), 341-347 (2004).
3. L. F. Pereira *et al.*, "Molybdenum Influence on the Mixed-Alkali Effect of Lithium–Sodium Phosphate Glasses," *J. Phys. Chem. C*, **122**(28), 15886-15891 (2018).
4. J. Swenson and S. Adams, "Mixed alkali effect in glasses," *Phys. Rev. Lett.*, **90**(15), 155507 (2003).
5. N. Vedeanu and D. Magdas, "The influence of some transition metal ions in lead-and calcium-phosphate glasses," *J. Alloys Compd.*, **534**, 93-96 (2012).
6. N. Mott, "Conduction in non-crystalline systems: IV. Anderson localization in a disordered lattice," *Philos. Mag. Lett.*, **22**(175), 7-29 (1970).
7. M. Hassan and C. Hogarth, "A study of the structural, electrical and optical properties of copper tellurium oxide glasses," *J. Mater. Sci.*, **23**(7), 2500-2504 (1988).
8. L. Abbas *et al.*, "Properties of mixed Li2O and Na2O molybdenum phosphate glasses," *J. Mol. Struct*," **876**(1-3), 194-198 (2008).
9. P. Maass, A. Bunde and M. D. Ingram, "Ion transport anomalies in glasses," *Phys. Rev. Lett.*, **68**(20), 3064 (1992).
10. A. Bunde, M. D. Ingram and P. Maass, "The dynamic structure model for ion transport in glasses," *J Non Cryst Solids*, **172**, 1222-1236 (1994).
11. A. Bunde, M. D. Ingram and S. Russ, "A new interpretation of the dynamic structure model of ion transport in molten and solid glasses," *Phys. Chem. Chem. Phys.*, **6**(13), 3663-3668 (2004).
12. J. Swenson *et al.*, "Structure of mixed alkali phosphate glasses by neutron diffraction and Raman spectroscopy," *Phys. Rev. B Condens. Matter*, **58**(17), 11331 (1998).
13. J. Swenson *et al.*, "Random ion distribution model: A structural approach to the mixed-alkali effect in glasses," *Phys. Rev. B Condens. Matter*, **63**(13), 132202 (2001).
14. A. Agarwal *et al.*, "Mixed alkali effect in optical properties of lithium–potassium bismuth borate glass system," *Mater. Lett.*, **58**(5), 694-698 (2004).
15. E. Davis and N. Mott, "Conduction in non-crystalline systems V. Conductivity, optical absorption and photoconductivity in amorphous semiconductors," *Philos. Mag. Lett*, **22**(179), 0903-0922 (1970).
16. M. Caglar, S. Ilican and Y. Caglar, "Influence of dopant concentration on the optical properties of ZnO: In films by sol–gel method," *Thin Solid Films*," **517(**17), 5023-5028 (2009).
17. D. Redfield, "Effect of defect fields on the optical absorption edge," *Phys. Rev.*, **130**(3), 916 (1963).

Technium Electro Vol. 1, pp.53-68 (2023)
ISSN:3008-6795
www.techniumscience.com

18. A. Kłonkowski, "Non-monotonic variations of some parameters in vitreous R2O SiO2 and R2O Al2O3 SiO2 systems," *J Non Cryst Solids*," **72**(1), 117-137 (1985).

Figures:

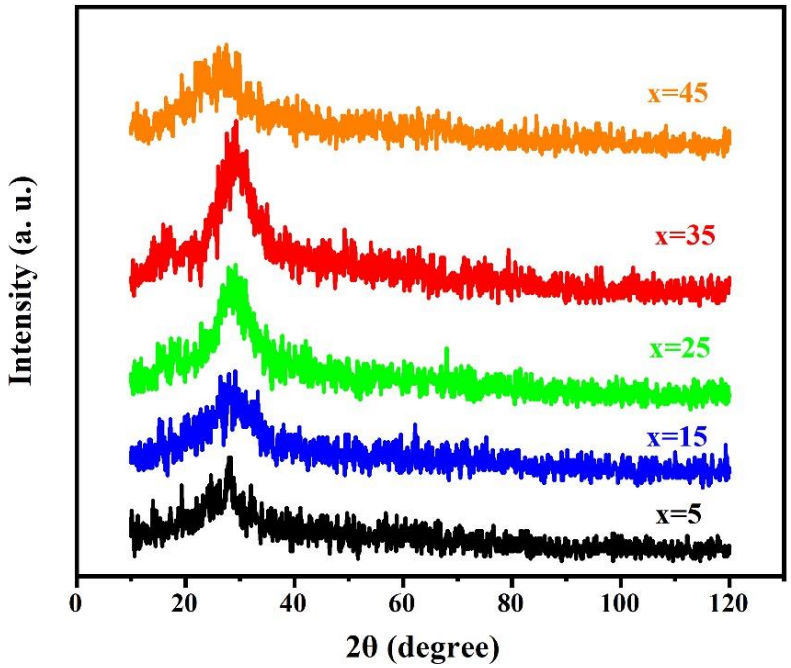

Fig. 1. XRD patterns of $40P_2O_5–10MnO_2–(50\text{-}x)Li_2O–xRb_2O$ glasses.

Technium Electro

Technium Electro Vol. 1, pp.53-68 (2023)
ISSN:3008-6795
www.techniumscience.com

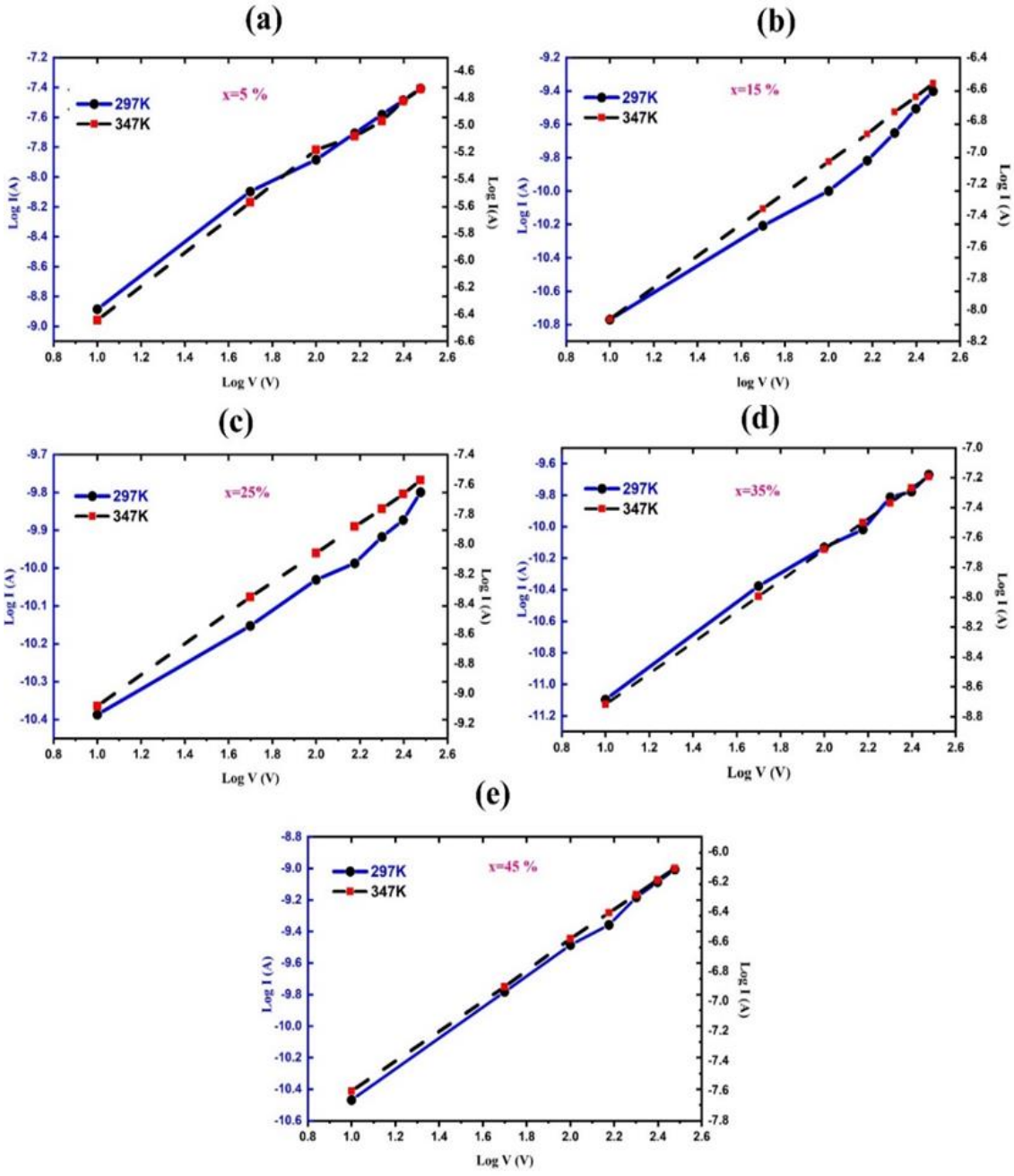

Fig. 2. A representative plot of Log (I) versus Log (V) at 297 K and 347 K for all vitreous samples.

Technium Electro Vol. 1, pp.53-68 (2023)
ISSN:3008-6795
www.techniumscience.com

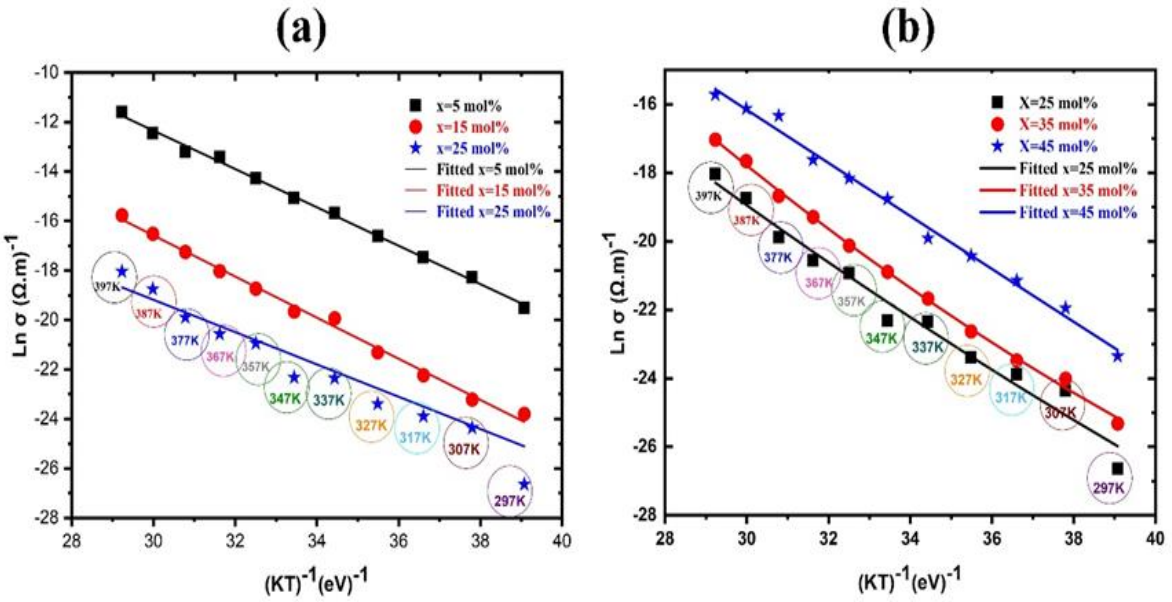

Fig. 3. Variation of dc electrical conductivity as a function of reciprocal temperature for all the samples.

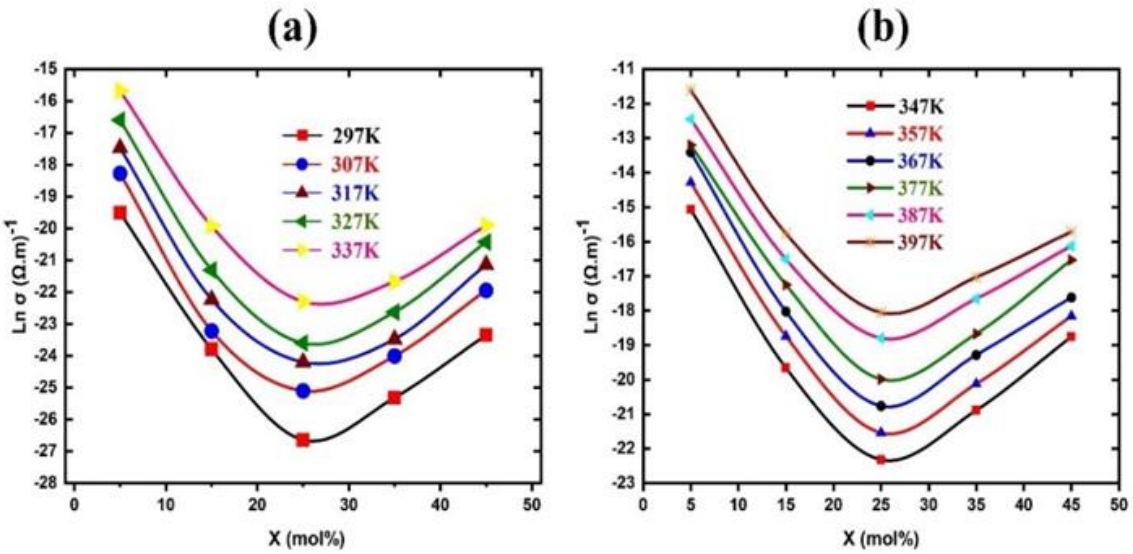

Fig. 4. Compositional dependence of dc electrical conductivity in the glassy samples.

Technium Electro Vol. 1, pp.53-68 (2023)
ISSN:3008-6795
www.techniumscience.com

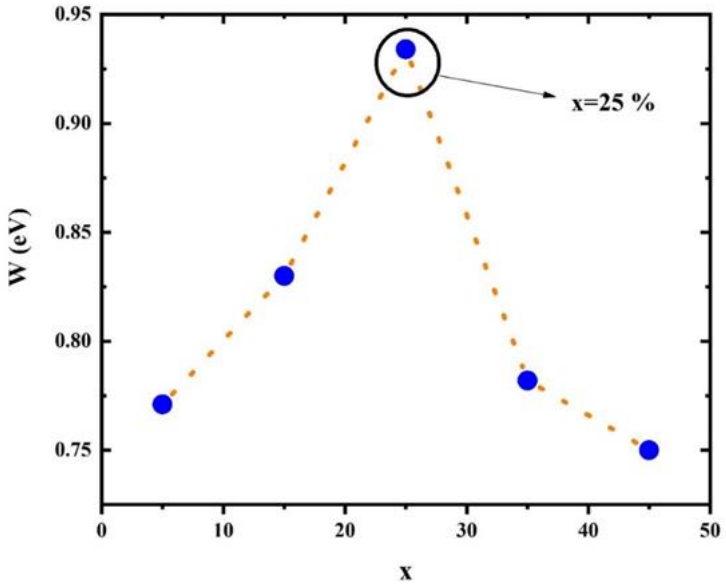

Fig. 5. Compositional dependence of activation energy.

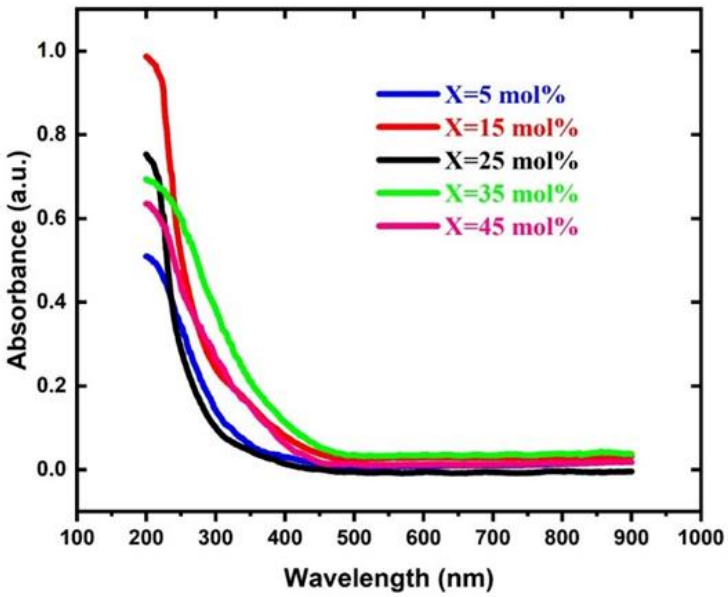

Fig. 6. Absorbance spectra for all vitreous samples.

Technium Electro

Technium Electro Vol. 1, pp.53-68 (2023)
ISSN:3008-6795
www.techniumscience.com

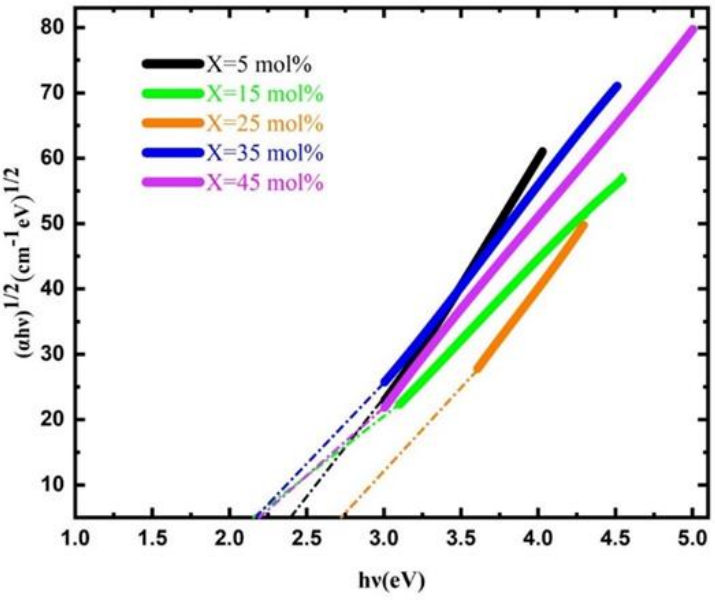

Fig. 7. Compositional and thermal dependence of dc electrical conductivity in the glassy samples.

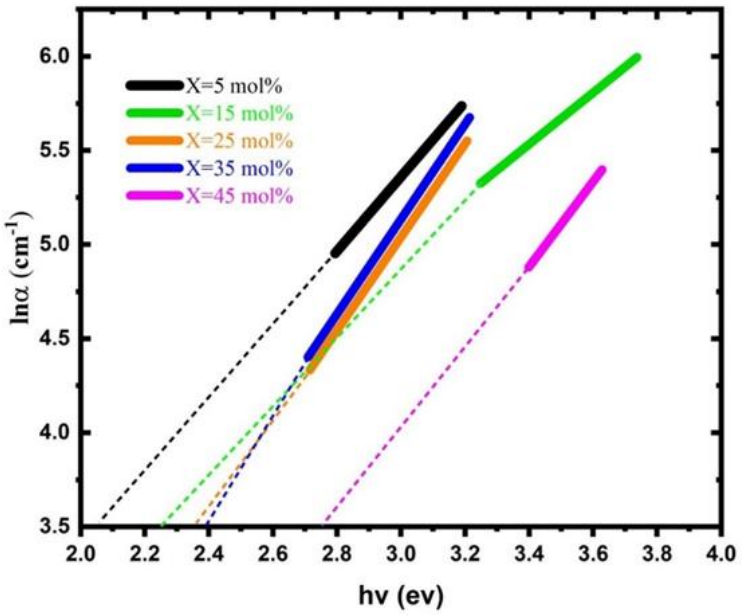

Fig. 8. The linear portion of Lnα versus incident photon energy.

Technium Electro

Technium Electro Vol. 1, pp.53-68 (2023)
ISSN:3008-6795
www.techniumscience.com

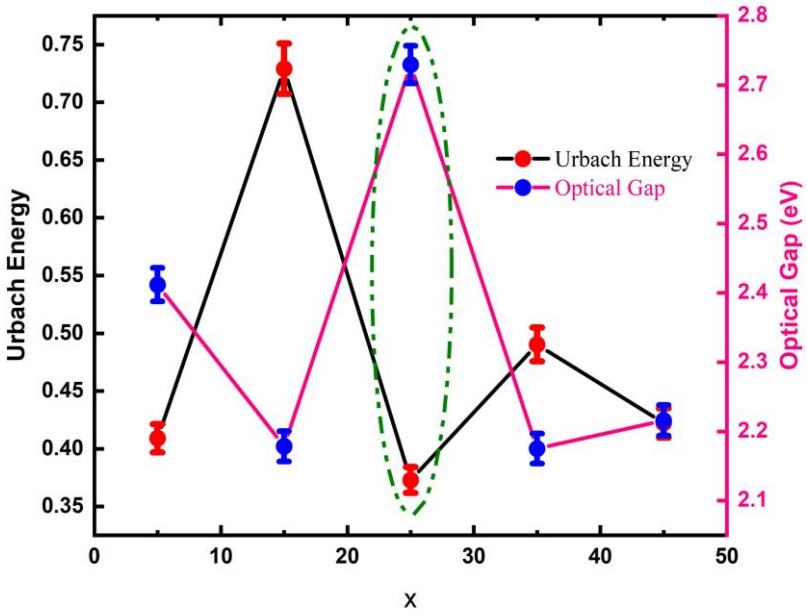

Fig. 9. Variation of optical bandgap and Urbach energy as a function of Rb_2O molar percentage in the composition of the glasses.

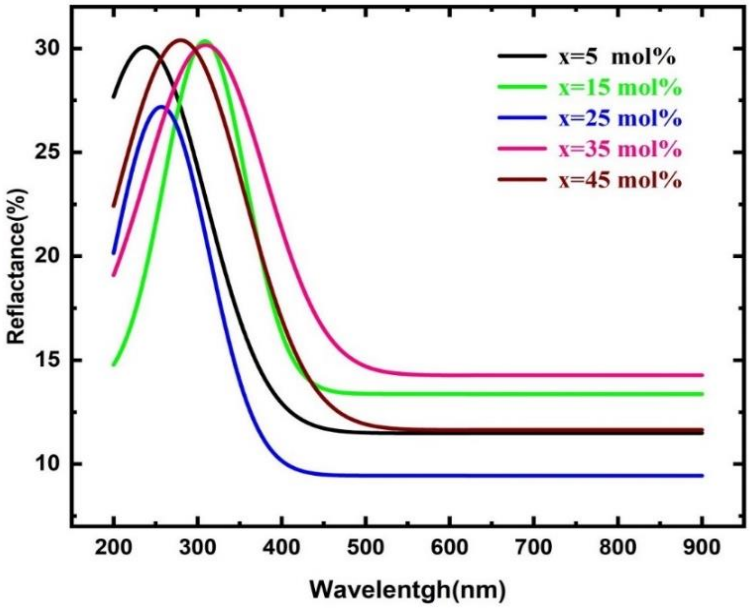

Fig. 10. Reflectance spectra for all the samples.

Technium Electro Vol. 1, pp.53-68 (2023)
ISSN:3008-6795
www.techniumscience.com

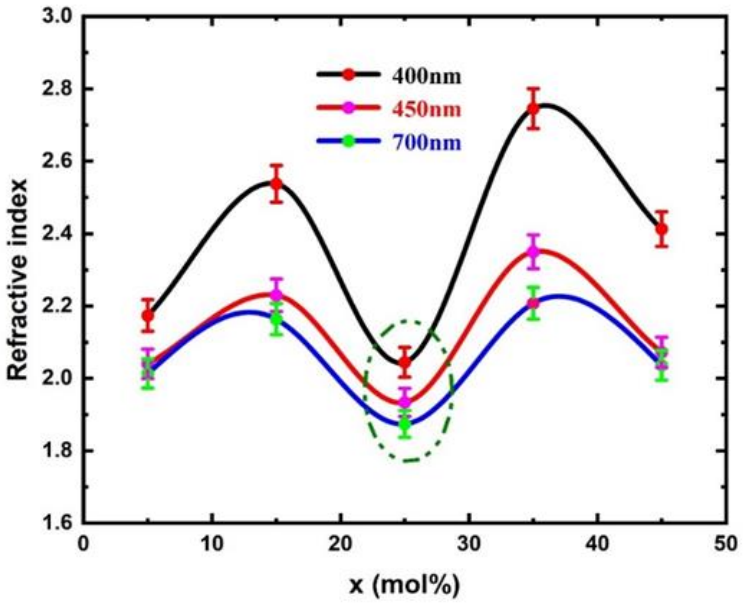

Fig. 11. Refractive index variation as a function of Rb_2O content (at λ= 400, 450 and 700 nm).

Tables:

TABLE 1. CAS Registry Number, Supplier, and Purity of the Chemicals.

Component	CAS RW. No.	Supplier	Purity
Ammonium dihydrogen phosphate	7722-76-1	Merck	99%
Manganese dioxide	1313-13-9	Merck	99%
Lithium carbonate	554-13-2	Merck	99.5%
Rubidium carbonate	584-09-8	Sigma	99.%

Technium Electro Vol. 1, pp.53-68 (2023)
ISSN:3008-6795
www.techniumscience.com

TABLE 2. Electrical Parameters for the Glassy Samples.

Parameters	**Glass composition**				
	x=5	**x=15**	**x=25**	**x=35**	**x=45**
Ln σ at 297K $(\Omega.m)^{-1}$ (±5%)	-19.711	-23.794	-26.641	-25.315	-23.353
Ln σ at 347K $(\Omega.m)^{-1}$ (±5%)	-15.064	-19.656	-22.326	-20.894	-18.763
W (eV) (±0. 01)	0.771	0.830	0.934	0.782	0.750

TABLE 3. Optical Parameters for the Glassy Samples.

Parameters	**Glass composition**				
	x=5	**x=15**	**x=25**	**x=35**	**x=45**
E_{opt} (eV)	2.411	2.178	2.729	2.175	2.215
E_U (eV)	0.412	0.721	0.374	0.492	0.425
n					
at λ=400nm	2.17	2.53	2.04	2.74	2.41
at λ=450nm	2.04	2.22	1.93	2.34	2.07
at λ=700nm	2.01	2.16	1.87	2.2	2.03
ε					
at λ=400nm	4.72	6.43	4.18	7.53	5.82
at λ=450nm	4.97	4.98	3.73	5.52	4.3
at λ=700nm	4.05	4.68	3.51	4.87	4.14
R					
at λ=400nm	0.079	0.11	0.06	0.13	0.025
at λ=450nm	0.066	0.084	0.056	0.096	0.069
at λ=700nm	0.063	0.078	0.5	0.082	0.083